REPORT DOCUMENTATION PAGE

Form Approved
OMB No. 0704-0188

1. REPORT DATE *(DD-MM-YYYY)*	2. REPORT TYPE	3. DATES COVERED *(From - To)*
10-02-2014	Final Technical Report	1 August 2011 - 31 January 2014

4. TITLE AND SUBTITLE
Structural Influence of Dynamics of Bottom Loads

5a. CONTRACT NUMBER

5b. GRANT NUMBER
N00014-11-1-0506

5c. PROGRAM ELEMENT NUMBER

6. AUTHOR(S)
Grenestedt, Joachim

5d. PROJECT NUMBER

5e. TASK NUMBER

5f. WORK UNIT NUMBER

7. PERFORMING ORGANIZATION NAME(S) AND ADDRESS(ES)
Lehigh University
526 Brodhead Avenue
Bethlehem, PA 18015

8. PERFORMING ORGANIZATION REPORT NUMBER

9. SPONSORING/MONITORING AGENCY NAME(S) AND ADDRESS(ES)
1- ONR REG. OFFICE CHICAGO N62880, 230 South Dearborn, Room 380, Chicago, IL 60604-1595; 2- Navy Research Laboratory, ATTN: CODE 5996, 455 Overlook Ave SW, Washington, DC 20375-5320; 3- Roshdy G. Barsoum, Office of Naval Research, 875 North Randolph Street, Arlington, VA 22203-1995; 4- Defense Technical Information Center, 8725 John J. Kingman Rd, Ste 0944, Fort Belvior, VA 22060-6218

10. SPONSOR/MONITOR'S ACRONYM(S)
ONR

11. SPONSOR/MONITOR'S REPORT NUMBER(S)

12. DISTRIBUTION/AVAILABILITY STATEMENT
Statement A: Approved for public release; distribution is unlimited

13. SUPPLEMENTARY NOTES

14. ABSTRACT
The deformation of boat hull bottom panels during the initial phase of slamming is studied analytically using a linear elastic Euler-Bernoulli beam as a representation of the cross section of a bottom panel. The slamming pressure is modeled as a high-intensity peak followed by a lower constant pressure, traveling at constant speed along the beam. The problem is solved using a Fourier sine integral transformation in space and a Laplace-Carson integral transformation in time. Deflection and bending moment as functions of time and position for different speeds, bending stiffnesses, etc. are given. In particular the effect of slamming load traveling speed on structural response of the simplified bottom structure is investigated. It is found that rather large deflections and bending moments are encountered at certain speeds of the pressure, which suggests that bottom panels may benefit from tailoring their stiffness and mass properties such that loads are reduced. This would vary with boat particulars and operation (deadrise angle, mass, speed, sea state, etc). The importance of the high-intensity pressure peak often encountered during slamming is also studied.

15. SUBJECT TERMS
Bottom slamming; Initial phase; Euler-Bernoulli beam; Two-step load, analytical method

16. SECURITY CLASSIFICATION OF: a. REPORT	b. ABSTRACT	c. THIS PAGE	17. LIMITATION OF ABSTRACT	18. NUMBER OF PAGES	19a. NAME OF RESPONSIBLE PERSON
			UU	31	Joachim Grenestedt
					19b. TELEPHONE NUMBER *(Include area code)* 610-758-4129

INSTRUCTIONS FOR COMPLETING SF 298

1. REPORT DATE. Full publication date, including day, month, if available. Must cite at least the year and be Year 2000 compliant, e.g. 30-06-1998; xx-06-1998; xx-xx-1998.

2. REPORT TYPE. State the type of report, such as final, technical, interim, memorandum, master's thesis, progress, quarterly, research, special, group study, etc.

3. DATES COVERED. Indicate the time during which the work was performed and the report was written, e.g., Jun 1997 - Jun 1998; 1-10 Jun 1996; May - Nov 1998; Nov 1998.

4. TITLE. Enter title and subtitle with volume number and part number, if applicable. On classified documents, enter the title classification in parentheses.

5a. CONTRACT NUMBER. Enter all contract numbers as they appear in the report, e.g. F33615-86-C-5169.

5b. GRANT NUMBER. Enter all grant numbers as they appear in the report, e.g. AFOSR-82-1234.

5c. PROGRAM ELEMENT NUMBER. Enter all program element numbers as they appear in the report, e.g. 61101A.

5d. PROJECT NUMBER. Enter all project numbers as they appear in the report, e.g. 1F665702D1257; ILIR.

5e. TASK NUMBER. Enter all task numbers as they appear in the report, e.g. 05; RF0330201; T4112.

5f. WORK UNIT NUMBER. Enter all work unit numbers as they appear in the report, e.g. 001; AFAPL30480105.

6. AUTHOR(S). Enter name(s) of person(s) responsible for writing the report, performing the research, or credited with the content of the report. The form of entry is the last name, first name, middle initial, and additional qualifiers separated by commas, e.g. Smith, Richard, J, Jr.

7. PERFORMING ORGANIZATION NAME(S) AND ADDRESS(ES). Self-explanatory.

8. PERFORMING ORGANIZATION REPORT NUMBER. Enter all unique alphanumeric report numbers assigned by the performing organization, e.g. BRL-1234; AFWL-TR-85-4017-Vol-21-PT-2.

9. SPONSORING/MONITORING AGENCY NAME(S) AND ADDRESS(ES). Enter the name and address of the organization(s) financially responsible for and monitoring the work.

10. SPONSOR/MONITOR'S ACRONYM(S). Enter, if available, e.g. BRL, ARDEC, NADC.

11. SPONSOR/MONITOR'S REPORT NUMBER(S). Enter report number as assigned by the sponsoring/ monitoring agency, if available, e.g. BRL-TR-829; -215.

12. DISTRIBUTION/AVAILABILITY STATEMENT. Use agency-mandated availability statements to indicate the public availability or distribution limitations of the report. If additional limitations/ restrictions or special markings are indicated, follow agency authorization procedures, e.g. RD/FRD, PROPIN, ITAR, etc. Include copyright information.

13. SUPPLEMENTARY NOTES. Enter information not included elsewhere such as: prepared in cooperation with; translation of; report supersedes; old edition number, etc.

14. ABSTRACT. A brief (approximately 200 words) factual summary of the most significant information.

15. SUBJECT TERMS. Key words or phrases identifying major concepts in the report.

16. SECURITY CLASSIFICATION. Enter security classification in accordance with security classification regulations, e.g. U, C, S, etc. If this form contains classified information, stamp classification level on the top and bottom of this page.

17. LIMITATION OF ABSTRACT. This block must be completed to assign a distribution limitation to the abstract. Enter UU (Unclassified Unlimited) or SAR (Same as Report). An entry in this block is necessary if the abstract is to be limited.

Structural Influence of Dynamics of Bottom Loads

Contract N000141110506

Joachim L. Grenestedt
Mechanical Engineering and Mechanics
P.C. Rossin College of Engineering and Applied Science
Lehigh University
Bethlehem, PA 18015, USA

Abstract: The deformation of boat hull bottom panels during the initial phase of slamming is studied analytically using a linear elastic Euler-Bernoulli beam as a representation of the cross section of a bottom panel. The slamming pressure is modeled as a high-intensity peak followed by a lower constant pressure, traveling at constant speed along the beam. The problem is solved using a Fourier sine integral transformation in space and a Laplace-Carson integral transformation in time. Deflection and bending moment as functions of time and position for different speeds, bending stiffnesses, etc. are given. In particular the effect of slamming load traveling speed on structural response of the simplified bottom structure is investigated. It is found that rather large deflections and bending moments are encountered at certain speeds of the pressure, which suggests that bottom panels may benefit from tailoring their stiffness and mass properties such that loads are reduced. This would vary with boat particulars and operation (deadrise angle, mass, speed, sea state, etc). The importance of the high-intensity pressure peak often encountered during slamming is also studied. It is seen that for relatively slow moving slamming loads the pressure peak has little influence. However, for faster moving loads its influence can be significant.

Keywords: Bottom slamming; Initial phase; Euler-Bernoulli beam; Two-step load, analytical method

1. Introduction

Some of the highest loads on high-speed boats are due to bottom slamming. Slamming pressures are very dynamic and vary significantly over the bottom. Typically slamming starts with a high-intensity pressure peak that travels rapidly over the bottom from the keel towards the chines. The pressure peak is usually followed by a lower and essentially constant pressure. The pressure peak magnitude and propagation speed depend heavily on the impact velocity and deadrise angle of the boat. Slamming peak pressures have been experimentally measured to reach 8 MPa or even more (e.g., Faltinsen [1]), which is close to the acoustic pressure (hammer pressure) for the vertical speeds studied. On the other hand current structural design criteria for high-speed craft treat slamming as static uniformly distributed pressures with considerably lower pressure magnitudes (e.g., DNV [2], ABS [3], Lloyds [4]). This raises the question whether the structures designed and manufactured by those criteria are conservative, over or under designed, or just plainly incorrectly designed. The present study tries to shed some light on this complex problem by analytically studying a simplified model of a bottom panel subjected to a non-uniform pressure distribution traveling at various speeds. More advanced studies, as well as correlation with experimentally measured slamming response using the Numerette research craft, are underway.

Early analytic research on slamming was done by von Karman [5] using a momentum approach, and by Wagner [6] using two-dimensional non-viscous incompressible flow. Cointe and Armand [7] studied the problem of an impacting cylinder and considered nonlinearity of the local jet flow. Zhao and Faltinsen [8] and Faltinsen [9] improved the solution of Wagner using a boundary element method and indicated a superposition of asymptotic expansions of high pressure at the spray root and a following lower pressure distribution. Faltinsen [9, 13] reported that hydroelastic effects are mainly relevant for local impacts when the deadrise angle is small and the duration of the impact is shorter or comparable to the structure's natural period. A conformal mapping technique was used by Mei et al. [10] to study the impact pressure on a two-dimensional body. Wet deck slamming was studied theoretically by Faltinsen [11] using a hydroelastic beam model. An initial structural inertia phase and a subsequent free vibration phase were identified. An asymptotic theory showed that the maximum bending stresses are proportional to an effective drop velocity and are not sensitive to the curvature of the wave surface or where the waves hit the beam.

Simply stated, slamming appears to consist of an initial slamming load arriving phase followed by a vibration phase. In this paper the bottom response during the slamming load arriving phase is analytically studied. The boat bottom is modeled as a one-dimensional linear elastic Euler-Bernoulli beam. The slamming pressure is modeled as a high intensity peak followed by a lower constant pressure, traveling at constant speed along the beam.

Fluid-structure interactions are at this time ignored, or simply included as a constant added-mass term. Air entrapment which may have a large influence at lower deadrise angles is also ignored. The deformation is assumed to be sufficiently small that linear-elastic beam theory is valid, and that the geometry of the deformed bottom is not significantly different from the undeformed one. The assumption that the load travels at constant speed across the beam in essence implies that the vertical velocity of the boat bottom is constant during the slamming event, which depending on boat particulars (geometry, mass, etc) may or may not be a reasonable assumption. The equations are solved by using a Fourier sine integral transformation in space and a Laplace-Carson integral transformation in time, as done by Fryba [12]. The structural response during the slamming load arriving phase is given. The effect of slamming load traveling speed on structural responses is presented.

2. Simplified Analytical Model of Slamming, Two-Step Load on Beam

Consider the system shown in Figure 1 in which a bottom panel is modeled as a simply supported Euler-Bernoulli beam subjected to the slamming load $q(x,t)$ which moves with constant velocity c from one end to the other. The model may be reasonably realistic for bottom panels which are long relative to their width, as is common in boat bottoms. Simply supported edges were chosen as a reasonable approximation of the bottom panels of the Numerette research craft. Its bottom consists of ten sandwich panels whose cores taper off and vanish by the edges, resulting in a single skin "collar" along the perimeter of each panel. The thin single skin collar is considerably more compliant in bending than the thick sandwich, thus modeling the edges as simply supported is presumably a decent approximation. It may or may not be a feasible approximation for the edges of bottom panels in other boats. The deflection of the beam is $w(x,t)$, where x ($0 \leq x \leq L$) is the position within the beam and t ($0 \le t \le L/c$) is time. In Figure 1, L is the length of the beam and l_1 is the length of the high-intensity pressure peak. The analysis in this paper terminates at $t=L/c$ when the pressure peak reaches the right end of the beam (corresponding to the slamming pressure reaching the chine of the boat).

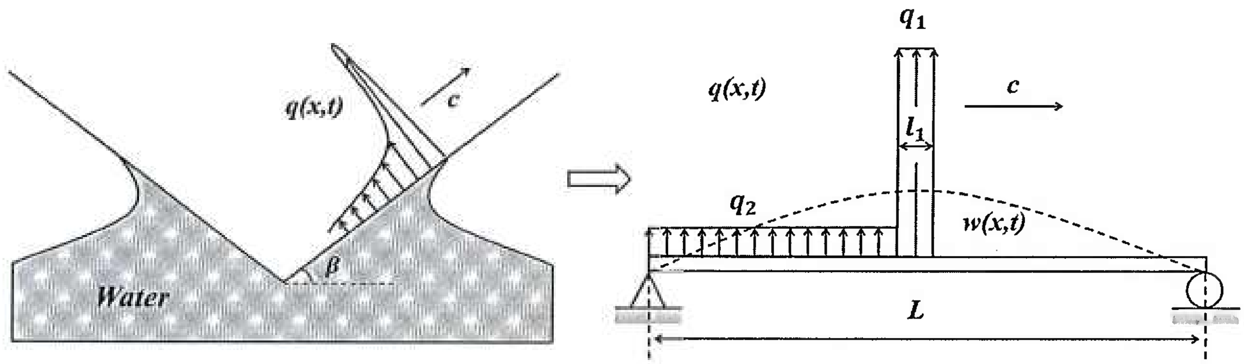

Figure 1. Left: cross-section of boat during slamming, showing the moving slamming pressure $q(x,t)$. Right: Simplified model where the bottom panel is represented by a beam and the slamming pressure $q(x,t)$ as two constant pressures, q_1 and q_2, traveling at a constant speed c.

Using the Euler-Bernoulli beam assumptions the governing equation is

$$EI\frac{\partial^4 w(x,t)}{\partial x^4} + \mu^* \frac{\partial^2 w(x,t)}{\partial t^2} = q(x,t) \tag{1}$$

where EI is bending stiffness (assumed constant), $q(x,t)$ is load per unit length, μ^* is total mass (mass of beam plus some added mass of water) per unit length of the beam (also assumed constant). The added mass of a submerged bottom panel is usually assumed to correspond to the mass of a half cylinder of water with diameter L and length d (in the present case d is the width of the beam). The total added mass is thus $\rho_w \pi L^2 d/8$. If it is assumed that this mass is evenly distributed along the length of the present beam, then the added mass per unit length becomes $\rho_w \pi L d/8$. This would be for a fully submerged panel, whereas at the beginning of the slamming event the bottom panel is essentially dry and there is no added mass term. For this reason a constant $k \in [0,1]$ was introduced, such that $\mu^* = \mu + k\rho_w \pi L d / 8$. For a fully submerged bottom panel k=1, whereas for a dry panel k=0; however in the analysis below k is assumed constant during the whole slamming event (from the time the keel touches the water surface to the time when the slamming pressure reaches the chine). It may be plausible to believe that the two cases k=0 and k=1 in some sense bound the behavior of a bottom panel.

In the present study the slamming load is simplified as a moving step load of the following form:

$$q(x,t) = q_1[1 - H(x - ct)] - (q_1 - q_2)[1 - H(x - c(t - l_1 / c))] \tag{2}$$

where q_1 is the load per unit length of the initial load peak, q_2 is the load per unit length of the residual load following the peak, and *H(x)* is the Heaviside step function,

$$H(x) = \begin{cases} 0 & \mathit{for} \quad x < 0 \\ 1 & \mathit{for} \quad x \geq 0 \end{cases} \tag{3}$$

Since equation (1) is linear, superposition applies and the problem can be solved in two parts. The first set of equations is

$$EI \frac{\partial^4 w(x,t)}{\partial x^4} + \mu^* \frac{\partial^2 w(x,t)}{\partial t^2} = q_1[1 - H(x - ct)] \tag{4}$$

The corresponding boundary conditions and the initial conditions for equation (4) are

$$w(0,t) = 0 \qquad\qquad w(L,t) = 0 \tag{5}$$

$$\left.\frac{\partial^2 w(x,t)}{\partial x^2}\right|_{x=0} = 0 \qquad \left.\frac{\partial^2 w(x,t)}{\partial x^2}\right|_{x=L} = 0$$

and

$$w(x,0) = 0 \qquad \left.\frac{\partial w(x,t)}{\partial t}\right|_{t=0} = 0 \tag{6}$$

The second set of equations is

$$EI\frac{\partial^4 w(x,t)}{\partial x^4} + \mu^* \frac{\partial^2 w(x,t)}{\partial t^2} = -(q_1 - q_2)[1 - H(x - c(t - l_1 / c))] \tag{7}$$

The corresponding boundary conditions and the initial conditions for equation (7) are

$$w(0,t) = 0 \qquad w(L,t) = 0 \tag{8}$$

$$\left.\frac{\partial^2 w(x,t)}{\partial x^2}\right|_{x=0} = 0 \qquad \left.\frac{\partial^2 w(x,t)}{\partial x^2}\right|_{x=L} = 0$$

and

$$\left. w(x,t)\right|_{t=l_1/c} = 0 \qquad \left.\frac{\partial w(x,t)}{\partial t}\right|_{t=l_1/c} = 0 \tag{9}$$

If $w(x,t)$ is the solution to the slamming problem, $w_1(x,t)$ is the solution to eqs. (4-6) and $w_2(x,t)$ is the solution to eqs. (7-9), then

$$w(x,t) = w_1(x,t) + w_2(x,t) \tag{10}$$

3. Nondimensionalization of the Problem

In order to reduce the number of parameters the following dimensionless quantities are introduced

$$\bar{x} = \frac{x}{L} \qquad \bar{l}_1 = \frac{l_1}{L} \qquad \bar{w} = \frac{w}{L} \qquad \bar{q} = \frac{L^3}{EI} q \qquad \bar{t} = t\sqrt{\frac{EI}{\mu^* L^4}}$$

$$\bar{c} = c\sqrt{\frac{\mu^* L^2}{EI}} \qquad \bar{M}(\bar{x},\bar{t}) = \frac{L}{EI} M(x,t) \tag{11}$$

The dimensionless versions of eqs. (4-6) are

$$\frac{\partial^4 \bar{w}(\bar{x},\bar{t})}{\partial \bar{x}^4} + \frac{\partial^2 \bar{w}(\bar{x},\bar{t})}{\partial \bar{t}^2} = \bar{q}_1\left[1 - H(\bar{x} - \bar{c}\bar{t})\right] \tag{12}$$

$$\bar{w}(0,\bar{t}) = 0 \qquad \bar{w}(1,\bar{t}) = 0 \tag{13}$$

$$\left.\frac{\partial^2 \bar{w}(\bar{x},\bar{t})}{\partial \bar{x}^2}\right|_{\bar{x}=0} = 0 \qquad \left.\frac{\partial^2 \bar{w}(\bar{x},\bar{t})}{\partial \bar{x}^2}\right|_{\bar{x}=1} = 0$$

and

$$\bar{w}(\bar{x},0) = 0 \qquad \left.\frac{\partial \bar{w}(\bar{x},\bar{t})}{\partial \bar{t}}\right|_{\bar{t}=0} = 0 \tag{14}$$

while the dimensionless versions of eqs. (7-9) are

$$\frac{\partial^4 \bar{w}(\bar{x},\bar{t})}{\partial \bar{x}^4} + \frac{\partial^2 \bar{w}(\bar{x},\bar{t})}{\partial \bar{t}^2} = -(\bar{q}_1 - \bar{q}_2)\left[1 - H(\bar{x} - \bar{c}(\bar{t} - \bar{l}_1/\bar{c}))\right] \tag{15}$$

$$\bar{w}(0,\bar{t}) = 0 \qquad \bar{w}(1,\bar{t}) = 0 \tag{16}$$

$$\left.\frac{\partial^2 \bar{w}(\bar{x},\bar{t})}{\partial \bar{x}^2}\right|_{\bar{x}=0} = 0 \qquad \left.\frac{\partial^2 \bar{w}(\bar{x},\bar{t})}{\partial \bar{x}^2}\right|_{\bar{x}=1} = 0$$

and

$$\left.\bar{w}(\bar{x},\bar{t})\right|_{\bar{t}=\bar{l}_1/\bar{c}} = 0 \qquad \left.\frac{\partial \bar{w}(\bar{x},\bar{t})}{\partial \bar{t}}\right|_{\bar{t}=\bar{l}_1/\bar{c}} = 0 \tag{17}$$

4. Solutions to the Equations

For equations (12-14), the solution $\bar{w}_1(\bar{x},\bar{t})$ can be obtained by using a Fourier sine integral transformation in space and a Laplace-Carson integral transformation in time [12]. Multiplying eq. (12) by $\sin j\pi\bar{x}$, where j is an integer, and integrating with respect to $\bar{x}$ between 0 and 1, using the boundary conditions (13) and relations (A1-A3) in Appendix A, the following is obtained:

$$j^4\pi^4 W(j,\bar{t}) + \ddot{W}(j,\bar{t}) = \frac{\bar{q}_1}{j\pi}(1-\cos j\pi\bar{c}\bar{t}) \qquad j = 1,2,3\cdots \tag{18}$$

where $W(j,\bar{t})$ is the Fourier sine integral transform of the original $\bar{w}_1(\bar{x},\bar{t})$,

$$W(j,\bar{t}) = \int_0^1 \bar{w}_1(\bar{x},\bar{t})\sin j\pi\bar{x}d\bar{x} \qquad j = 1,2,3\cdots \tag{19}$$

$$\overline{w}_1(\overline{x},\overline{t}) = 2\sum_{j=1}^{\infty} W(j,\overline{t}) \sin j\pi\overline{x} \tag{20}$$

Set $a = j^2\pi^2$ and $b = j\pi\overline{c}$, then equation (18) can be reorganized as follows

$$\ddot{W}(j,\overline{t}) + a^2 W(j,\overline{t}) = \frac{\overline{q}_1}{j\pi}(1-\cos b\overline{t}) \qquad j = 1,2,3\cdots \tag{21}$$

Next we apply the Laplace-Carson integral transformation on equation (21), i.e. multiply each term in eq. (21) by $e^{-s\overline{t}}$, integrate with respect to $\overline{t}$ between 0 and ∞, and multiply by s which is a variable in the complex plane. Using the initial conditions (14) and relations (B1-B3) in Appendix B, we can get

$$W^*(j,s) = \frac{\overline{q}_1}{j\pi} \frac{b^2}{(s^2+a^2)(s^2+b^2)} \tag{22}$$

where $W^*(j,s)$ is the Laplace-Carson transform of the original $W(j,\overline{t})$,

$$W^*(j,s) = s\int_0^{\infty} W(j,\overline{t}) e^{-s\overline{t}} d\overline{t} \tag{23}$$

Applying the inverse Laplace-Carson transformation on equation (22), using relations (B2) (B4), the solution is obtained,

$$W(j,\overline{t}) = \frac{\overline{q}_1}{j^5\pi^5}\left[1 + \frac{1}{a^2-b^2}(b^2\cos a\overline{t} - a^2\cos b\overline{t})\right] \tag{24}$$

This solution is not valid if $a=b$, i.e. when $j=\pi\bar{c}$. However, this can be avoided by a slight change in $\bar{c}$, and therefore will be tacitly ignored.

With equation (20) and (24), we shall get the solution to eqs. (12-14), where $0 \le \bar{t} \le 1/\bar{c}$ and $0 \le \bar{x} \le 1$,

$$\bar{w}_1(\bar{x},\bar{t}) = \frac{2\bar{q}_1}{\pi^5}\sum_{j=1}^{\infty}\frac{1}{j^5}\left[1+\frac{1}{a^2-b^2}\left(b^2\cos a\bar{t} - a^2\cos b\bar{t}\right)\right]\sin j\pi\bar{x}, \quad a = j^2\pi^2,\ b = j\pi\bar{c} \tag{25}$$

The solution to the second set of equations, eqs. (15-17), is obtained by a time shift and scaling,

$$\bar{w}_2(\bar{x},\bar{t}) = \begin{cases} 0 & (0 \le \bar{t} \le \frac{\bar{l}_1}{\bar{c}}) \\ \frac{2(\bar{q}_2-\bar{q}_1)}{\pi^5}\sum_{j=1}^{\infty}\frac{1}{j^5}\left[1+\frac{1}{a^2-b^2}(b^2\cos a(\bar{t}-\frac{\bar{l}_1}{\bar{c}}) \right. & \\ \qquad \left. - a^2\cos b(\bar{t}-\frac{\bar{l}_1}{\bar{c}})\right]\sin j\pi\bar{x} & (\frac{\bar{l}_1}{\bar{c}} \le \bar{t} \le \frac{1}{\bar{c}}) \end{cases} \tag{26}$$

Thus, the final solution for a moving step load is

$$\bar{w}(\bar{x},\bar{t}) = \begin{cases} \frac{2\bar{q}_1}{\pi^5}\sum_{j=1}^{\infty}\frac{1}{j^5}\left[1+\frac{1}{a^2-b^2}\left(b^2\cos a\bar{t} - a^2\cos b\bar{t}\right)\right]\sin j\pi\bar{x} & (0 \le \bar{t} \le \frac{\bar{l}_1}{\bar{c}}) \\ \frac{2}{\pi^5}\sum_{j=1}^{\infty}\frac{1}{j^5}\left[\bar{q}_2+\frac{\bar{q}_1}{a^2-b^2}\left(b^2\cos a\bar{t} - a^2\cos b\bar{t}\right)\right. & \\ \qquad \left. -\frac{\bar{q}_1-\bar{q}_2}{a^2-b^2}\left(b^2\cos a(\bar{t}-\frac{\bar{l}_1}{\bar{c}}) - a^2\cos b(\bar{t}-\frac{\bar{l}_1}{\bar{c}})\right)\right]\sin j\pi\bar{x} & (\frac{\bar{l}_1}{\bar{c}} \le \bar{t} \le \frac{1}{\bar{c}}) \end{cases} \tag{27}$$

With the deflection known other quantities of interest, like the bending moment or the shear forces in the beam, are easily obtained. In particular, the bending moment is

$$M = -EI\frac{\partial^2 w(x,t)}{\partial x^2}, \quad \overline{M} = -\frac{\partial^2 \overline{w}(\overline{x},\overline{t})}{\partial \overline{x}^2} \tag{28}$$

and thus

$$\overline{M}(\overline{x},\overline{t}) = \begin{cases} \dfrac{2\overline{q}_1}{\pi^3}\displaystyle\sum_{j=1}^{\infty}\frac{1}{j^3}\left[1+\frac{1}{a^2-b^2}\left(b^2\cos a\overline{t} - a^2\cos b\overline{t}\right)\right]\sin j\pi\overline{x} & (0 \le \overline{t} \le \dfrac{\overline{l}_1}{c}) \\ \dfrac{2}{\pi^3}\displaystyle\sum_{j=1}^{\infty}\frac{1}{j^3}\left[\overline{q}_2 + \frac{\overline{q}_1}{a^2-b^2}\left(b^2\cos a\overline{t} - a^2\cos b\overline{t}\right)\right. & \\ \quad \left. -\dfrac{\overline{q}_1-\overline{q}_2}{a^2-b^2}\left(b^2\cos a(\overline{t}-\dfrac{\overline{l}_1}{c}) - a^2\cos b(\overline{t}-\dfrac{\overline{l}_1}{c})\right)\right]\sin j\pi\overline{x} & (\dfrac{\overline{l}_1}{c} \le \overline{t} \le \dfrac{1}{c}) \end{cases} \tag{29}$$

In the next section a slightly different pressure profile will be discussed.

5. Alternative Pressure Distribution, the Point-Step Load

As mentioned measurements of bottom pressures in high-speed boats indicate that there is a high pressure peak spreading rapidly over the bottom, followed by a considerably lower pressure over a large area of the bottom. The pressure peak was represented by the pressure (times width) q_1 above. The importance of the pressure peak can be further studied by representing it by a moving point-load, F_D, followed by a constant pressure. This will be called the "Point-Step Load" in the remainder of the paper. The normalized slamming load $\overline{q}(\overline{x},\overline{t})$ can then be expressed as

$$\overline{q}(\overline{x},\overline{t}) = \overline{F}_D\delta\left(\overline{x}-\overline{ct}\right) + \overline{q}_r[1-H(\overline{x}-\overline{ct})] \tag{30}$$

where $\delta(x)$ is a Dirac pulse and $\overline{q}_r$ is a residual pressure following the point load. In order to compare this load with the two-step load, the point-load load is set equal to the total load of the initial peak, and the total load when the slamming reaches the right end of the beam is made the same for the two different loads; thus

$$\overline{F}_D = \overline{q}_1 \overline{l}_1 \qquad \overline{q}_r = \overline{q}_2 (1 - \overline{l}_1) \tag{31}$$

The governing equation for this load is

$$\frac{\partial^4 \overline{w}_I(\overline{x},\overline{t})}{\partial \overline{x}^4} + \frac{\partial^2 \overline{w}_I(\overline{x},\overline{t})}{\partial \overline{t}^2} = \overline{F}_D \delta(\overline{x} - \overline{c}\overline{t}) + \overline{q}_r \left[1 - H(\overline{x} - \overline{c}\overline{t})\right] \tag{32}$$

together with the boundary and initial conditions, eqs. (13-14). The problem is solved in a similar fashion as for the two-step load, and with the help of (A4), (B4) and (B5) the solution becomes:

$$\begin{aligned} \overline{w}_I(\overline{x},\overline{t}) = {} & 2\pi \overline{F}_D \overline{c} \sum_{j=1}^{\infty} \frac{j}{a^2 - b^2} \left(\frac{1}{b} \sin b\overline{t} - \frac{1}{a} \sin a\overline{t} \right) \sin j\pi\overline{x} \\ & + \frac{2\overline{q}_r}{\pi^5} \sum_{j=1}^{\infty} \frac{1}{j^5} \left[1 + \frac{1}{a^2 - b^2} \left(b^2 \cos a\overline{t} - a^2 \cos b\overline{t} \right) \right] \sin j\pi\overline{x} \end{aligned} \tag{33}$$

$$\begin{aligned} \overline{M}_I(\overline{x},\overline{t}) = {} & 2\pi^3 \overline{F}_D \overline{c} \sum_{j=1}^{\infty} \frac{j^3}{a^2 - b^2} \left(\frac{1}{b} \sin b\overline{t} - \frac{1}{a} \sin a\overline{t} \right) \sin j\pi\overline{x} \\ & + \frac{2\overline{q}_r}{\pi^3} \sum_{j=1}^{\infty} \frac{1}{j^3} \left[1 + \frac{1}{a^2 - b^2} \left(b^2 \cos a\overline{t} - a^2 \cos b\overline{t} \right) \right] \sin j\pi\overline{x} \end{aligned} \tag{34}$$

With the definition of the point load and the residual pressure of eq. (31), the total load at the time the slamming reaches the right end of the beam is the same for this load as for the two-step load. However, at any other time the total force is higher for the present pressure distribution.

6 Convergence and Error Analysis

In this section the errors introduced by terminating the infinite series solutions of eqs. (27) and (29) are studied. With some rearrangement of eq. (25) the following is obtained,

$$\begin{aligned}\left|\bar{w}_1(\bar{x},\bar{t})\right| &\le \left|\frac{2\bar{q}_1}{\pi^5}\right|\sum_{j=1}^{\infty}\frac{1}{j^5}+\left|\frac{2\bar{q}_1\bar{c}^{-2}}{\pi^5}\right|\sum_{j=1}^{\infty}\left|\frac{1}{j^5\left(j^2\pi^2-\bar{c}^{-2}\right)}\right|+\left|\frac{2\bar{q}_1}{\pi^3}\right|\sum_{j=1}^{\infty}\left|\frac{1}{j^3\left(j^2\pi^2-\bar{c}^{-2}\right)}\right| \\ &\le \left|\frac{2\bar{q}_1}{\pi^5}\right|\sum_{j=1}^{J_1-1}\frac{1}{j^5}+\left|\frac{2\bar{q}_1\bar{c}^{-2}}{\pi^5}\right|\sum_{j=1}^{J_1-1}\left|\frac{1}{j^5\left(j^2\pi^2-\bar{c}^{-2}\right)}\right|+\left|\frac{2\bar{q}_1}{\pi^3}\right|\sum_{j=1}^{J_1-1}\left|\frac{1}{j^3\left(j^2\pi^2-\bar{c}^{-2}\right)}\right| \\ &\quad +\left|\frac{2\bar{q}_1\left(1+\bar{c}^{-2}\right)}{\pi^5}\right|\sum_{j=J_1}^{\infty}\frac{1}{j^5}+\left|\frac{2\bar{q}_1}{\pi^3}\right|\sum_{j=J_1}^{\infty}\frac{1}{j^3}\end{aligned} \tag{35}$$

where J_1 is an integer equal or greater than $\sqrt{1+\bar{c}^{-2}}/\pi$ (so $j^2\pi^2-\bar{c}^{-2}\ge 1$). Since a p-series with $p>1$ is convergent, the solution $\bar{w}_1(\bar{x},\bar{t})$ is also convergent (except if $j=\pi\bar{c}$, which as mentioned previously is disregarded).

For numerical calculations a truncated series is used,

$$\bar{w}_1^c(\bar{x},\bar{t})=\frac{2\bar{q}_1}{\pi^5}\sum_{j=1}^{J_1-1}\frac{1}{j^5}\left[1+\frac{1}{a^2-b^2}\left(b^2\cos a\bar{t}-a^2\cos b\bar{t}\right)\right]\sin j\pi\bar{x} \tag{36}$$

with an error limited by

$$\begin{aligned}\left|error\right|_d &=\left|\frac{2\bar{q}_1}{\pi^5}\sum_{j=J_1}^{\infty}\frac{1}{j^5}\left[1+\frac{1}{a^2-b^2}\left(b^2\cos a\bar{t}-a^2\cos b\bar{t}\right)\right]\sin j\pi\bar{x}\right| \\ &\le \left|\frac{2\bar{q}_1\left(1+\bar{c}^{-2}\right)}{\pi^5}\right|\sum_{j=J_1}^{\infty}\frac{1}{j^5}+\left|\frac{2\bar{q}_1}{\pi^3}\right|\sum_{j=J_1}^{\infty}\frac{1}{j^3}\end{aligned} \tag{37}$$

Since

$$\sum_{j=J_1}^{\infty}\frac{1}{j^5}<\int_{J_1-1}^{\infty}\frac{1}{x^5}dx=\frac{1}{4(J_1-1)^4} \quad \text{and} \quad \sum_{j=J_1}^{\infty}\frac{1}{j^3}<\int_{J_1-1}^{\infty}\frac{1}{x^3}dx=\frac{1}{2(J_1-1)^2} \tag{38}$$

the error estimate becomes

$$|error|_d<\left|\frac{\bar{q}_1\left(1+\bar{c}^2\right)}{2\pi^5(J_1-1)^4}\right|+\left|\frac{\bar{q}_1}{\pi^3(J_1-1)^2}\right| \tag{39}$$

Similarly, for the bending moment $\overline{M}_1=-\dfrac{\partial^2\overline{w}_1(\bar{x},\bar{t})}{\partial\bar{x}^2}$, we can get the following result

$$\overline{M}_1^c(\bar{x},\bar{t})=\frac{2\bar{q}_1}{\pi^3}\sum_{j=1}^{J_2-1}\frac{1}{j^3}\left[1+\frac{1}{a^2-b^2}\left(b^2\cos a\bar{t}-a^2\cos b\bar{t}\right)\right]\sin j\pi\bar{x} \tag{40}$$

where J_2 is an integer equal or greater than $\left(1+\sqrt{1+4\pi^2\bar{c}^2}\right)/2\pi^2$. An upper bound of the error of the bending moment $\overline{M}_1^c(\bar{x},\bar{t})$ is

$$|error|_m<\left|\frac{\bar{q}_1}{\pi^3(J_2-1)^2}\right|+\left|\frac{2\bar{q}_1\bar{c}^2}{3\pi^3(J_2-1)^3}\right|+\left|\frac{2\bar{q}_1}{\pi(J_2-1)}\right| \tag{41}$$

7 Range of Parameters for Slamming

Slamming calculations will in this paper be performed for parameters that are relevant for boats and ships. The speed that the slamming load travels over the bottom, c, can be estimated by

$$c = \frac{V\pi}{2\tan\beta} \cdot \frac{1}{\cos\beta} = \frac{V\pi}{2\sin\beta} \tag{42}$$

where V is the vertical velocity of a 2D wedge dropped in water and β is the deadrise angle of the bottom, e.g., Faltinsen [13]. It will be assumed that deadrise angles of the boats of interest are in the range 5° to 45°, and the vertical velocity in the range 1 m/s to 10 m/s. Drop tests with these parameters have been performed in [1], [14] and [16]. Using these values the speed that the slamming load travels over the bottom, c, is estimated by eq. [42] to vary from 2 m/s to 200 m/s. Peak pressure and duration were deduced from among other sources the drop tests of [1], [14] and [16]. The peak pressure range and peak duration in Table 1 appears to cover the majority of such tests. The ratio of p_1/p_2 is naturally not clearly defined from experiments since real slamming loads differs from the two-step load presently assumed. However, for the purpose of presenting results the pressure ratio p_1/p_2 was assumed to be in the range of 2~20.

Table 1. Range of parameters studied

Parameters	Traveling load speed c [m/s]	Peak pressure [kPa]	ratio of p_1/p_2	Duration of slamming load peak [ms]
Value Ranges	2~200	10~8,000	2~20	0.01~2

Regarding bottom stiffness, the range can be estimated to vary from that of a very soft bottom panel such as a one meter wide 3 mm thick aluminum plate (E=70 GPa, density 2700 kg/m^3), to a stiff bottom such as a one meter wide sandwich panel with two 15 mm thick carbon fiber skins (E=100 GPa, density 1500 kg/m^3) on each side of a 70 mm thick high density foam core (negligible stiffness, density 250 kg/m^3). This results in a bending stiffness (EI) ratio of the soft bottom to the stiff bottom of approximately 3×10^{-5}. With this ratio, the ranges of interest of the dimensionless parameters given in Table 2 are obtained (from eq. (11)). The length l_1 was estimated as traveling load speed times duration of the pressure peak, resulting in the normalized length $\bar{l}_1$ of Table 2 if the length of the beam is 1 m.

Table 2. Range of interest of the dimensionless parameters

Parameters	Traveling load speed $\bar{c}$	Peak pressure $\bar{q}_1$	Ratio of $\bar{q}_1/\bar{q}_2$	Peak load length $\bar{l}_1$
Value Ranges	0.01~320	10^{-3}~10^{5}	2~20	2×10^{-5}~0.4

In the next section dynamic deflection $\bar{w}$ and bending moment $\bar{M}$ will be presented. They will be normalized by the maximum static deflection $\bar{w}_{ms}$ and the maximum static bending moment $\bar{M}_{ms}$ that result if the beam is statically subjected to a two-step load with the same properties as the dynamic load (i.e., as in Figure 1). Let $\bar{x}=a$ be the right edge of the pressure pulse $\bar{q}_1$. Then

$$\bar{w}_{ms} = \max_{0<a<1,0<x<1}\left|\bar{w}_s\right| \qquad \bar{M}_{ms} = \max_{0<a<1,0<x<1}\left|\bar{M}_s\right| \tag{43}$$

where $\overline{w}_s$ and $\overline{M}_s$ are the normalized static deflection and bending moment, respectively; please see Appendix C for more details.

8 Results and Discussion

A sample calculation will reveal some of the features of dynamically loaded bottom panels. Consider a simply supported beam subjected to a moving slamming load with the following parameters: $\bar{c}=5, \bar{q}_1/\bar{q}_2=5$, $\bar{l}_1=0.01$. The deflections at four instances ($\bar{t}=\frac{1}{4\bar{c}},\frac{1}{2\bar{c}},\frac{3}{4\bar{c}}$ and $\frac{1}{\bar{c}}$) are shown in Figure 2, and the bending moments are shown in Figure 3. The vertical axes represent the deflection ratio $\overline{w}/\overline{w}_{ms}$ and the bending moment ratio $\overline{M}/\overline{M}_{ms}$, respectively. In this example the Point-Step Load predicts slightly higher deflection and bending moment of the beam in most instances, as would be expected. In this case the maximum deflection reaches approximately 55% of the maximum static deflection. The fact that the load is moving thus reduced the maximum deflection in this case. This is not generally true as will be seen shortly.

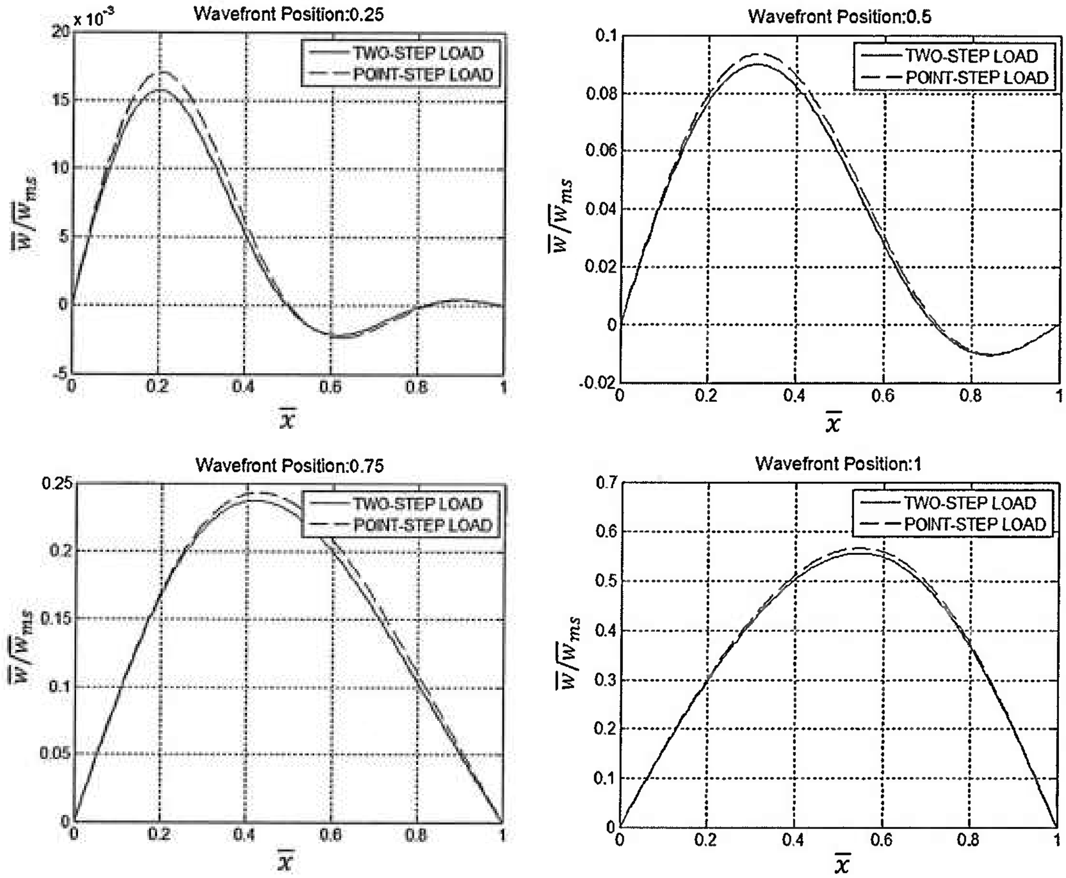

Figure 2. Deflection ratio $\overline{w}/\overline{w}_{ms}$ of the beam under moving slamming load with $\overline{c}=5$, $\overline{q}_1/\overline{q}_2=5$, $\overline{l}_1=0.01$

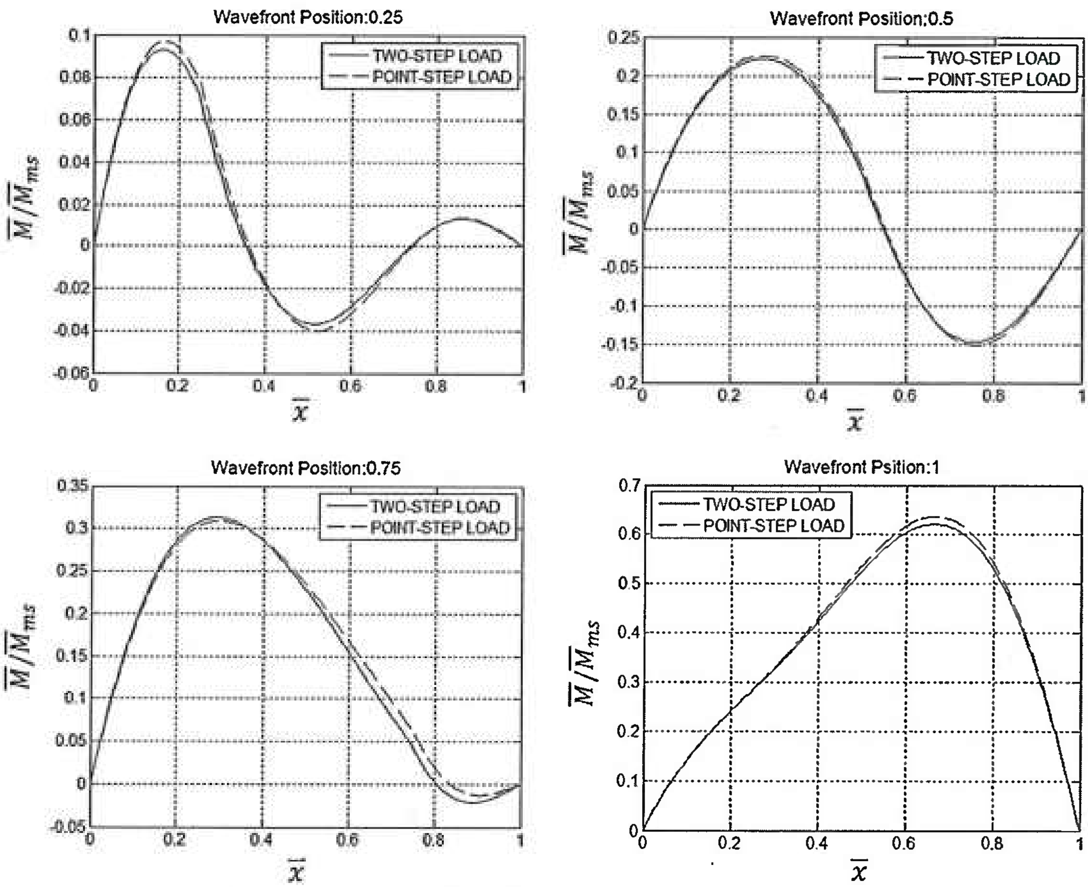

Figure 3. Bending moment ratio $\overline{M} / \overline{M}_{ms}$ of the beam under moving slamming load with $\bar{c}=5$, $\bar{q}_1 / \bar{q}_2 = 5$, $\bar{l}_1 = 0.01$

The effects of the slamming load traveling speed on structural responses are sketched in Figures 4 and 5 when $\bar{l}_1 = 0.01$. They show the maximum absolute value of the dynamic deflection and bending moment,

$$\bar{w}_{md} = \max_{0<\bar{t}<1/\bar{c},0<\bar{x}<1} |\bar{w}| \qquad \overline{M}_{md} = \max_{0<\bar{t}<1/\bar{c},0<\bar{x}<1} |\overline{M}| \tag{44}$$

normalized by the maximum static deflection, $\bar{w}_{ms}$, and the maximum static bending moment, $\overline{M}_{ms}$, respectively. Note that $\bar{w}_{md}$ and $\overline{M}_{md}$ depend on $\bar{c}$, while $\bar{w}_{ms}$ and $\overline{M}_{ms}$ do not. The results in Figures 4 and 5 demonstrate an important phenomenon of the structural response during the slamming load arriving phase. When the dimensionless slamming load moving speed is relatively low, the maximum dynamic deflection and moment are close to their static counterparts, as expected. However, for the present case with $\bar{l}_1 = 0.01$, when $\bar{c}$ increases to around 2 the maximum dynamic deflection is approximately 50% higher than the maximum static deflection. The same is true for the bending moment, the dynamic bending moment is approximately 50% higher than the static one. There is a form of resonance occurring in the structure. Considerable vibrations are occurring during the slamming load arriving phase when $\bar{c}$ is relatively low. From equations (1) and (8) the eigenfrequencies of a simply supported Euler-Bernoulli beam can be easily found: $\omega_i = \frac{\pi^2 i^2}{L^2}\sqrt{\frac{EI}{\mu^*}}, (i = 1,2,3\cdots)$. If we define a characteristic velocity as $c_i = \frac{L\omega_i}{2\pi}$, then the dimensionless characteristic velocity will be $\bar{c}_i = \frac{\pi i^2}{2}$. The first three dimensionless characteristic velocities are 1.6, 6.3 and 14.1. The two lower graphs in Figures 4 and 5 indicate that when $\bar{l}_1 = 0.01$ the most severe structural response occurs when the propagation speed $\bar{c}$ is slightly higher than the first characteristic velocity. Faltinsen [11] also pointed out that maximum strains occur during the free vibration phase and mainly the lowest eigenmode is of importance at the time scale when maximum strains occur.

Presumably due to inertia effects, at higher propagation speed $\bar{c}$ the maximum deflection and bending moment, $\bar{w}_{md}$ and $\bar{M}_{md}$, decrease rapidly. When $\bar{c}$ is larger than the third characteristic velocity, 14.1, the maximum structure response ratios, $\bar{w}_{md} / \bar{w}_{ms}$ and $\bar{M}_{md} / \bar{M}_{ms}$, are rather small. This is referred to as the inertia phase by Faltinsen [11], and implies that the slamming force is essentially balanced by structural inertia forces. After the inertia phase, the structure starts to vibrate with an initial velocity obtained at the end of the inertia phase. For $\bar{c}$ larger than 40, the maximum dynamic deflection and bending moment at the end of the slamming load arriving phase is less than 10% of the corresponding maximum static values.

Some effect of varying the peak pressure ratio, $\bar{q}_1 / \bar{q}_2$, is also illustrated in Figures 4 and 5. With $\bar{l}_1 = 0.01$, increasing the pressure ratio from 1 to 20 leads to higher deflection and bending moment ratios, $\overline{w}_{md} / \overline{w}_{ms}$ and $\overline{M}_{md} / \overline{M}_{ms}$. In other words, a slamming load with the same peak pressure but higher pressure ratio will result in a more severe structural response compared with the corresponding static response.

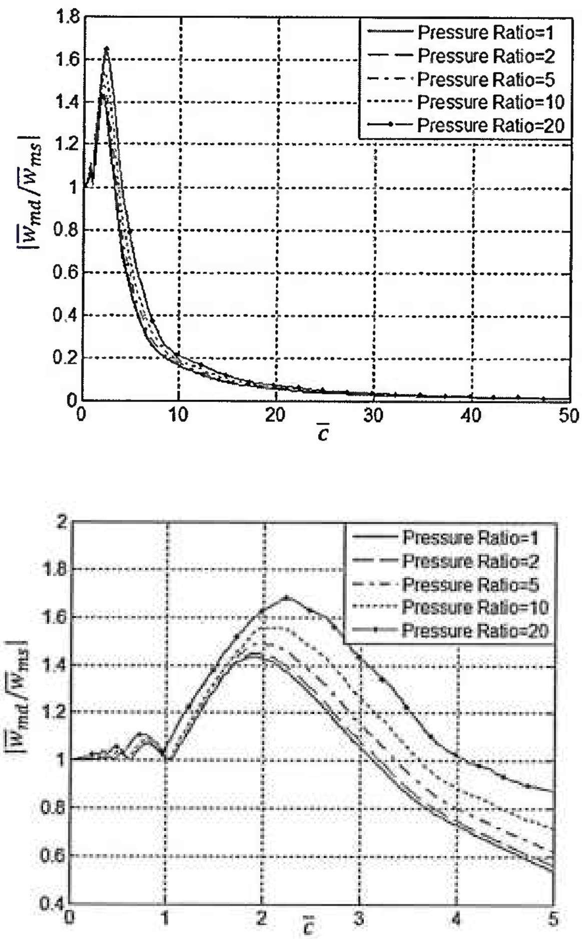

Figure 4. Maximum deflection ratio versus speed of the slamming load for five different pressure ratios $\overline{q}_1 / \overline{q}_2$ when $\overline{l}_1 = 0.01$. The lower graph is a zoomed-in version of the upper graph.

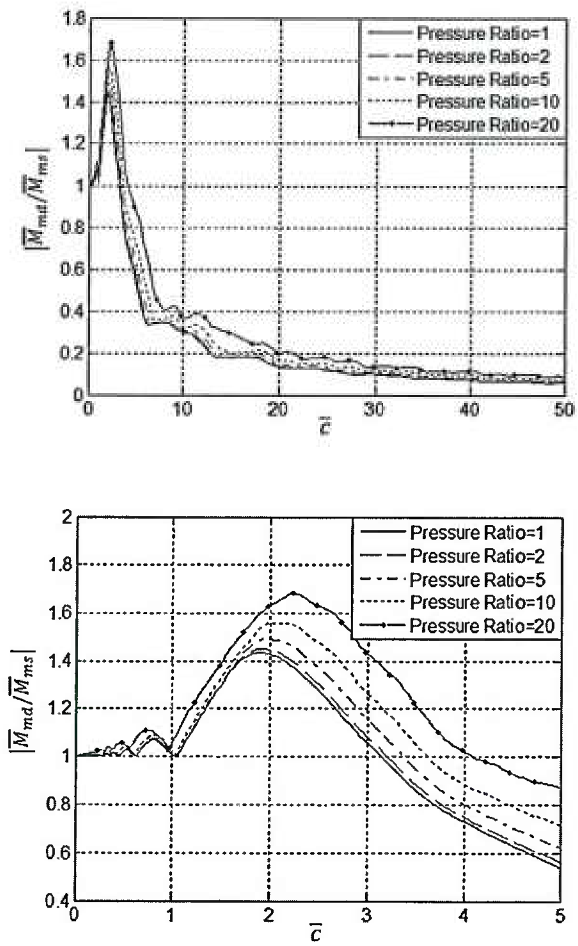

Figure 5. Maximum bending moment ratio versus speed of the slamming load for five different pressure ratios $\overline{q}_1 / \overline{q}_2$ when $\overline{l}_1 = 0.01$. The lower graph is a zoomed-in version of the upper graph.

An effect of peak load length, $\bar{l}_1$, is shown in Figures 6 and 7 for $\bar{q}_1/\bar{q}_2 = 5$. Three different $\bar{l}_1$ were used, 0.001, 0.01 and 0.1. The deflections and bending moments were normalized by their static equivalents as before in this paper. The figures indicate that both the normalized maximum deflection and dynamic bending moment increase with increasing peak load length, $\bar{l}_1$. Hence, slamming load with long duration of the peak pressure appears to generate more deflection and bending moment compared with the static equivalents.

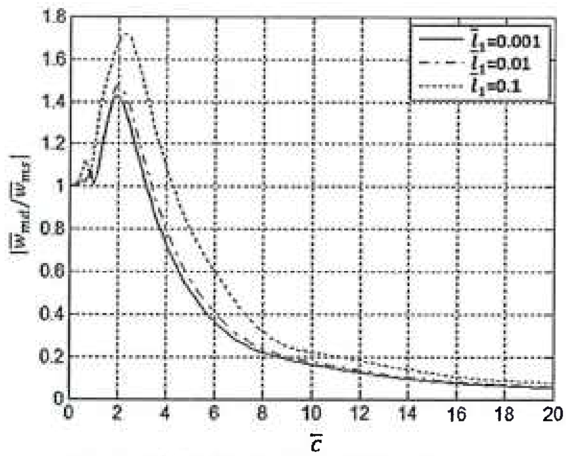

Figure 6. Maximum deflection ratio versus speed of the slamming load for three different $\bar{l}_1$, when $\bar{q}_1/\bar{q}_2 = 5$

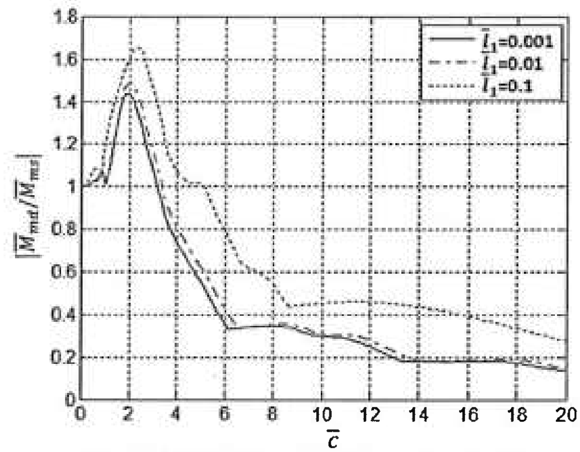

Figure 7. Maximum bending moment ratio versus speed of the slamming load for three different $\bar{l}_1$, when $\bar{q}_1/\bar{q}_2 = 5$

Some further insight into slamming can be gained by studying the influence of the total force of the initial peak pressure. The Point-Step load outlined previously was used for this purpose, i.e., a point load F_D preceding a constant pressure q_r. The maximum dynamic deflection and the maximum dynamic bending moment were calculated for different point loads F_D. In this case the deflection was normalized by the static deflection of a beam loaded by a distributed pressure q_r only, i.e., by $\bar{w}_s = \left|5\bar{q}_r/384\right|$. Likewise, the dynamic bending moment was normalized by $\bar{M}_s = \left|\bar{q}_r/8\right|$. The results are presented in Figures 8 and 9 where deflection and bending moment are plotted versus F_D/q_rL.

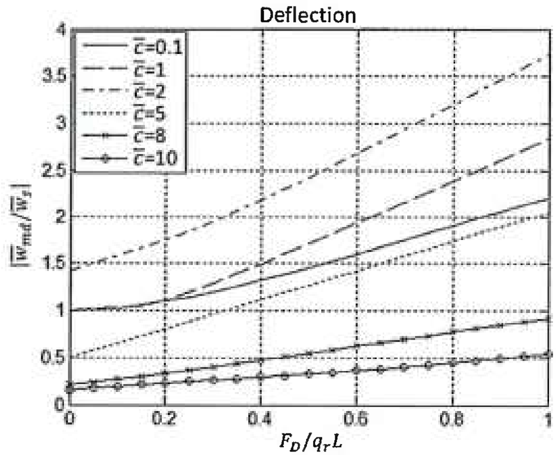

Figure 8. Maximum deflection versus point force ratio, normalized by maximum deflection from static evenly distributed load q_r.

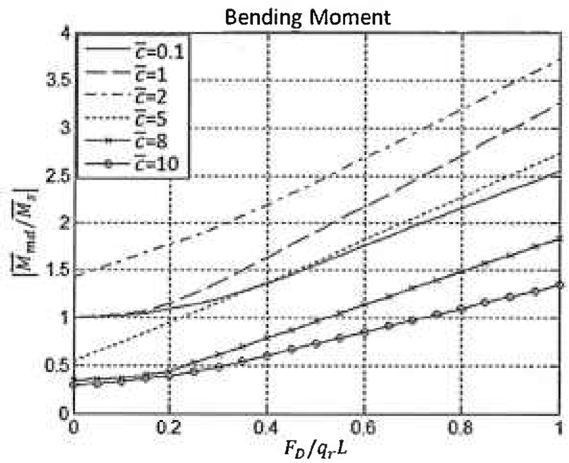

Figure 9. Maximum bending moment versus point force ratio, normalized by maximum moment from static evenly distributed load q_r.

Figure 8 and 9 show that the maximum deflection and bending moment of the structure increase monotonously with increasing point force ratio, $F_D / q_r L$, as expected. Further, as previously seen when $\bar{c}$ is close to the first characteristic velocity, 1.6, the maximum deflection and the maximum bending moment of the structure are the largest. After this high deflection and high bending moment phase, $\overline{w}_{md}$ and $\overline{M}_{md}$ decrease with increasing speed of the slamming load. Further, the figures indicate that reasonably small point loads have only little effect on the structural response when the slamming load travels slowly. For example, the increase in deflection and bending moment is just a few percent (relative to $\overline{w}_s$ and $\overline{M}_s$) for $F_D / q_r L = 0.1$ and $\bar{c} = 0.1$ or $\bar{c} = 1$. However, at higher speeds, such as $\bar{c} = 2$ or $\bar{c} = 5$, the increase is quite considerable. For $\bar{c} = 2$ the increase in deflection and bending moment over $\overline{w}_s$ and $\overline{M}_s$ is approximately 12 % while for $\bar{c} = 5$ the deflection increased 31% and the bending moment 38% in spite of the fact that the total load is only 10 % higher because of the point load.

9 Conclusions

The initial phase of slamming was studied using a simplified beam model subjected to moving loads. At slow speed of the moving load the maximum dynamic deflection and the maximum dynamic bending moment do not differ much from their static counterparts, but when the speed approaches a characteristic speed of the panel the maximum deflection and bending moment increase on the order of 50 %. At speeds above a few times the characteristic speed, the maximum deflection and bending moment decrease below the static values (during the initial phase under study). Both keep decreasing monotonically as the speed increases. This suggests that bottom panels could be tailored to avoid large deflections and bending moments. In particular panel stiffnesses could be avoided for which the characteristic speed of the panel is near the propagation speed of the slamming load. Granted, this may be difficult, or even impossible, to achieve for any speed and any sea state for a particular boat. Nevertheless, it may be possible to design a boat's bottom such that the effects of the most severe condition (speed, sea state) are reduced. It should further be noted that the speed and the pressure of the moving load depend on deadrise angle of the hull; for example reducing the deadrise angle would increase the speed of the slamming load (which may be beneficial) but also the pressure (which would not be beneficial). More analyzes using more refined models would be required to gain a better understanding of the potential of tailoring bottom panels for slamming.

The leading edge of the slamming pressure is typically characterized by a high pressure peak. If the force in this peak is on the order of 10% of the total force on the bottom panel, then at slow slamming load propagation speeds (less than, say, half the characteristic speed of the panel) this pressure peak does not increase maximum deflection or maximum bending moment significantly. However, at higher speeds (on the order of three times the characteristic speed) the maximum deflection and maximum bending moment increase 30-40% due to this pressure peak (compared to the response from a static evenly distributed load with no pressure peak), which is very significant.

REFERENCES

[1] Odd M. Faltinsen, Hydroelastic slamming, J. Mar. Sci. Tech., 5(2) (2000) 49-65.

[2] Det Norske Veritas (DNV), Rules for High Speed, Light Craft and Naval Surface Craft, Pt.3 Ch.1 Sec.2 pp. 14, July 2012.

[3] American Bureau of Shipping (ABS), Rules for Building and Classing High-Speed Craft, Pt. 3 Ch.2 Sec.2 pp. 57, 2013.

[4] Germanischer Lloyd (GL), Rules & Guidelines, I-Pt.3 Ch.1 pp. 3-17, 2012.

[5] Von Karman, The impact on seaplane floats during landing, Technical report 321,NACA, (1929).

[6] Wagner H, Uber stoss und gleitvorgänge an der oberfläche von flüssigkeiten, ZAMM 12 (1932) 193-215.

[7] Cointe R., Armand J., Hydrodynamic impact analysis of a cylinder, ASME, J. Offshore Mech. Arct. Eng., 109 (1987) 237-243.

[8] Zhao R., Odd M. Faltinsen, Water entry of two-dimensional bodies, J. Fluid. Mech. 246 (1993) 593-612.

[9] Odd M. Faltinsen, Water entry of a wedge by hydroelastic orthotropic plate theory, J. Ship Res., 43 (1999) 180-193.

[10] Mei X., Lui Y., Yue D. K. P., On the water impact of general two-dimensional sections, Appl. Ocean Res., 21 (1999) 1-15.

[11] Odd M. Faltinsen, The effect of hydroelasticity on ship slamming, Phil. Trans. R. Soc. A., 355 (1997) 1-17.

[12] L. Fryba, Vibration of Solids and Structures under Moving Loads, 3rd edition, Telford, 1999.

[13] Odd M. Faltinsen, Hydrodynamics of High-Speed Marine Vehicles, Cambridge University Press, New York, 2005, pp.308-309.

[14] B. Peseux, L. Gornet, B. Donguy, Hydrodynamic impact: Numerical and experimental investigations, J. Fluids. Struct. 21 (2005) 277-303.

[15] Nabanita Datta, Hydroelastic response of marine structures to impact-induced vibrations, The University of Michigan, Dissertation, 2010.

[16] G. K. Kapsenberg, Slamming of ships: where are we now?, Phil. Trans. R. Soc. A 369 (2011) 2892–2919.

Appendix A

Fourier sine integral transformation

Equation NO.	Original $f(x)$	Transform $F(j)$
A1	$\frac{d^4 f(x)}{dx^4}$ for $f(0)=f(L)=f''(0)=f''(L)=0$	$\frac{j^4\pi^4}{L^4}F(j)$
A2	$\sum_{i=1}^{n} a_i f_i(x)$	$\sum_{i=1}^{n} a_i F_i(j)$
A3	$b[1-H(x-a)]$	$\frac{bL}{j\pi}\left(1-\cos\frac{j\pi a}{L}\right)$
A4	$\delta(x-a)$	$\sin\frac{j\pi a}{L}$

Appendix B

Laplace-Carson integral transformation

Equation NO.	Original $f(t)$	Transform $F(s)$
B1	$\frac{d^2 f(t)}{dt^2}$	$s^2F(s)-s^2f(0_+)-s\frac{df(0_+)}{dt}$
B2	$\sum_{i=1}^{n} a_i f_i(t)$	$\sum_{i=1}^{n} a_i F_i(s)$
B3	$1-\cos at$	$\frac{a^2}{s^2+a^2}$
B4	$\frac{1}{a^2b^2}\left[1+\frac{1}{a^2-b^2}(b^2\cos at-a^2\cos bt)\right]$	$\frac{1}{(s^2+a^2)(s^2+b^2)}$

B5	$\frac{1}{a}\sin at$	$\frac{s}{s^2+a^2}$

Appendix C

The dynamic moment is normalized by the maximum static moment. The maximum static moment within the beam depends on where the (slamming) load is applied. Introduce the distance a such that the right end of the load q_1 in Figure 1 is located at $x=a$. In the dynamic case $a=ct$. The maximum static bending moment cannot occur for $a<l_1$ since additional load will increase the maximum moment. For $a>l_1$ the bending moment in a beam that is statically loaded as in Figure 1 is

$$M=\begin{cases} -\dfrac{q_2x^2}{2}+\dfrac{\left(l_1^2q_1-2al_1q_1+2Ll_1q_1-a^2q_2+2al_1q_2-l_1^2q_2+2Laq_2-2Ll_1q_2\right)x}{2L} & , \quad 0<x\le a-l_1 \\ -\dfrac{q_1x^2}{2}+\dfrac{\left(l_1^2q_1-2al_1q_1+2Laq_1-a^2q_2+2al_1q_2-l_1^2q_2\right)x}{2L}-\dfrac{\left(a-l_1\right)^2\left(q_1-q_2\right)}{2} & , \quad a-l_1<x\le a \\ \dfrac{\left(l_1^2q_1-2al_1q_1-a^2q_2+2al_1q_2-l_1^2q_2\right)x}{2L}-\dfrac{\left(l_1^2q_1-2al_1q_1-a^2q_2+2al_1q_2-l_1^2q_2\right)}{2} & , \quad a<x\le L \end{cases}$$

The maximum moment can occur either when $a=l_1$, when $a=L$, or when $l_1<a<L$. In either case, since $M(0)=M(L)=0$ and M and its slope are continuous, the maximum moment will be found where $dM/dx=0$. The three different cases are:

Case 1, $a=l_1$

$$M^1=\begin{cases} -\dfrac{q_1x^2}{2}+\dfrac{\left(2Ll_1-l_1^2\right)q_1x}{2L} & , \quad 0<x<l_1 \\ -\dfrac{l_1^2q_1x}{2L}+\dfrac{l_1^2q_1}{2} & , \quad l_1<x<L \end{cases}$$

The maximum moment for this case is

$$M^1_{\max}=\frac{l_1^2\left(2L-l_1\right)^2q_1}{8L^2}$$

Case 2, $l_1<a<L$

The maximum will be in the range $0<x<a$ since for $x>a$ the derivative dM/dx is never zero. The maximum moment will be found in the range $x<a-l_1$ if

$$l_1 < \bar{l}_1 \equiv \frac{aq_1 - Lq_1 - aq_2 + \sqrt{a^2q_1^2 - 2aLq_1^2 + L^2q_1^2 - a^2q_1q_2 + 2aLq_1q_2}}{q_1 - q_2}$$

and otherwise in the range $a-l_1< x<a$. The maximum moment is

$$M^2_{\max} = \begin{cases} \dfrac{\left(-l_1(l_1+2L)(q_1-q_2)+a^2q_2+2a\left(l_1(q_1-q_2)-Lq_2\right)\right)^2}{8L^2q_2} & \text{if} \quad l_1<\bar{l}_1 \\ \dfrac{\left(2al_1q_1-l_1^2q_1+a^2q_2-2al_1q_2+l_1^2q_2\right)\left(2al_1q_1-l_1^2q_1-4aLq_1+4L^2q_1+a^2q_2-2al_1q_2+l_1^2q_2\right)}{8L^2q_1} & \text{if} \quad l_1>\bar{l} \end{cases}$$

Case 3, $a=L$

The moment is

$$M^3 = \begin{cases} -\dfrac{q_2x^2}{2}+\dfrac{\left(l_1^2q_1-l_1^2q_2+L^2q_2\right)x}{2L} & , \quad 0\le x\le L-l_1 \\ -\dfrac{q_1x^2}{2}+\dfrac{\left(l_1^2q_1-2Ll_1q_1+2L^2q_1-L^2q_2+2Ll_1q_2-l_1^2q_2\right)x}{2L}-\dfrac{(L-l_1)^2(q_1-q_2)}{2} & , \quad L-l_1<x\le L \end{cases}$$

The maximum moment will be found where dM/dx=0, which is in the range $x<L-l_1$ if

$$l_1 < \frac{L}{\sqrt{q_1/q_2}+1}$$

and otherwise in the range $x>L-l_1$. The maximum moment is

$$M_{\max}^3 = \begin{cases} \dfrac{\left(l_1^2(q_1 - q_2) + L^2 q_2\right)^2}{8L^2 q_2} & \text{if} \quad 0 < l_1 < \dfrac{L}{\sqrt{q_1 / q_2} + 1} \\ \dfrac{\left((2Ll_1 - l_1^2)(q_1 - q_2) + L^2 q_2\right)^2}{8L^2 q_1} & \text{if} \quad L > l_1 > \dfrac{L}{\sqrt{q_1 / q_2} + 1} \end{cases}$$

Total

The maximum moment is the maximum of M^1, M^2, and M^3,

$$M_{ms} = \max[M_{\max}^1, M_{\max}^2, M_{\max}^3]$$